Journal of Thermal Analysis, Vol. 25 (1982) 473–485

PHASES FORMED DURING THE THERMAL ANALYSIS OF PYRITE IN AIR

F. R. A. JORGENSEN and F. J. MOYLE

CSIRO Division of Mineral Chemistry, P. O. Box 124, Port Melbourne, Victoria 3207, Australia

(Received February 3, 1982)

The oxidation of pyrite was studied by thermal analysis and quenching of the phases formed at different stages of the reaction. The phases were characterized by optical microscopy, SEM, EDAX, XRD and microprobe analyses. The phases found were essentially those predicted assuming thermodynamic and pressure equilibria. The predictions were that (1) below 404 °C hematite would form directly on the pyrite surface whereas at higher temperatures magnetite would intervene, (2) pyrrhotite would become a stable phase above 552 °C, (3) ferrous and ferric sulphates would form in the outer layers at temperatures below 583 and 644 °C respectively. The ignition temperature of pyrite was found to correspond with the onset of pyrrhotite formation. An arrest in some of the TG traces was ascribed to the presence of sulphates, the presence or absence of the arrest depending upon the temperature rise sustained by the sample during oxidation.

There is general agreement [1–13] that the final product of the oxidation of pyrite in air is ferric oxide, usually hematite. Kopp and Kerr [8] mentioned the possible formation of γ-ferric oxide and Banerjee [2] has identified this material in X-ray diffraction (XRD) patterns. Agreement as to the intermediate phases is not unanimous. Pyrrhotite was claimed to be present, or hinted at as a possibility, by many workers [3–5, 7–9, 11, 12, 14] but it was searched for by Banerjee [2] using XRD and chemical means and Schorr and Everhart [6] using XRD alone, and reported absent. Similarly, although magnetite was claimed to be present by several workers [4, 5, 8, 9, 11], Schwab and Philinis [13] could not detect it by XRD. Wustite has not been identified, though its presence was alluded to by Blachere [7] and there were mentions of its formation during the oxidation of pyrrhotite, [13, 15]. Sulphate has been claimed to be present, either as the ferrous [2, 4, 5, 16–17] or ferric forms [2, 13], but Schorr and Everhart [6] using high-temperature XRD found no evidence of sulphates. Similarly Niwa and Wada [12], who also used XRD techniques, were unable to find evidence of sulphates. Banerjee [2], claims to have identified a small amount of basic sulphate by chemical means.

There is a need, therefore, to examine the phases formed during the oxidation of pyrite to resolve some of the controversy noted above. This was accomplished in the present study by

a) using sensitive thermal analysis techniques to provide information on weight changes and heat effects accompanying the oxidation,

b) developing quenching techniques which enabled samples to be taken at any temperature during thermal analysis,

c) characterizing the phases formed, by optical and scanning electron microscopy (SEM), energy dispersive analysis (EDAX), XRD and microprobe traverses, and

d) conducting a thermodynamic analysis.

Experimental

Materials

Various size fractions were prepared by screening pyrite flotation concentrate from Mount Morgan in Queensland. Most of the work reported here used the average 53 – 74 μm screen size fraction. This was relatively pure pyrite containing traces of copper and zinc, and 0.7% silica. Compressed air was dried by passage over magnesium perchlorate.

Equipment and methods

Simultaneous differential thermal analysis (DTA) and thermogravimetric analysis (TG) were carried out using a Rigaku "Thermoflex" analyser. The initial samples and final residues were weighed using a Perkin Elmer microbalance. Pt-Pt 13% Rh thermocouples were used to measure the reference and sample temperatures. Flowing air atmospheres were used in most experiments. To minimize gas diffusion effects, small sample weights (2 mg) and shallow crucibles (4 mm dia. × 2 mm high – internal dimensions) were used. For these conditions, the sample approximated single-layer coverage of the bottom of the crucible.

Where material was required for phase identification and examination, the samples were heated in the furnace of the thermal analysis equipment and then quenched in liquid nitrogen. The crucible containing the sample hung in the furnace on a platinum support which was attached by a platinum wire to a cotton thread which left the apparatus by the top gas entry tube and was secured external to the apparatus. Maintenance of the air atmosphere within the furnace was ensured by a thin film of polyethylene which closed the bottom of the furnace and separated it from the nitrogen atmosphere in the flask. Air flowed down the furnace tube and exited at the bottom through a pinhole in the polyethylene. At the end of the desired time, the experiment was terminated by cutting the cotton thread. This allowed the hot crucible to fall, pierce the polyethylene, and enter the liquid nitrogen.

Close correspondence between the quenching experiments and the thermal analysis experiments was ensured by holding the sample in the same position in the furnace under the same experimental conditions of sample weight, heating rate and air flow. In the quenching experiments there was no thermocouple to measure the sample temperature; for these experiments, where it was desired to heat to a known final temperature, the time of the heating programme was determined from a normal thermal analysis experiment. When the liquid nitrogen had evaporated the sample was recovered by washing it from the flask carbon tetrachloride. This avoided possible hydrolysis of sulphates.

Results

Thermal analysis

The records of thermal analysis were reproducible; the traces were, however, sensitive to the experimental conditions. Figures 1 and 2 show the two extremes in

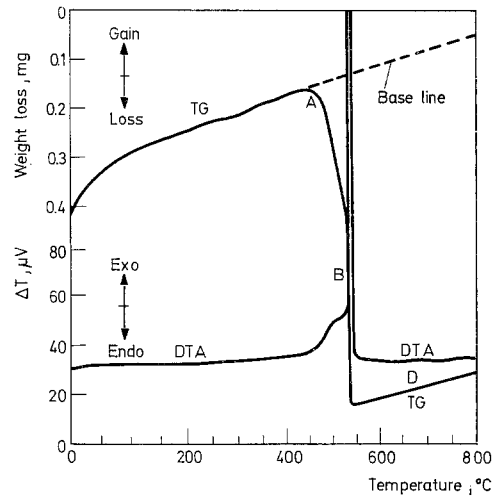

Fig. 1. Typical thermal analysis record of pyrite in air — TG arrest absent (sample wt 2.30 mg, particle size 53—74 μm, heating rate 10° min^{-1}, air flow rate 150 cm^3 min^{-1}, silica crucible. See text for significance of letters

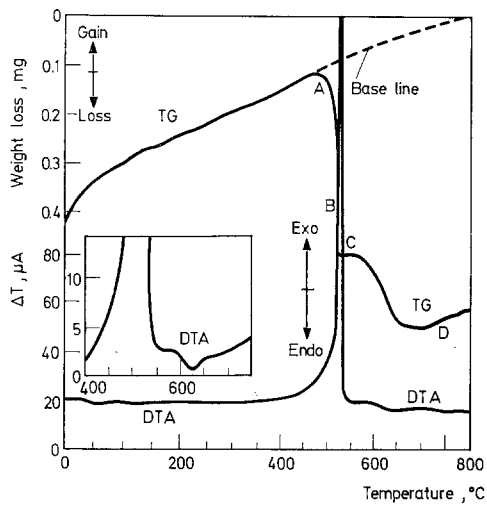

Fig. 2. Typical thermal analysis record of pyrite in air — TG arrest present (sample wt 2.06 mg particle size 53—74 μm, heating rate 10° min^{-1}, air flow rate 150 cm^3 min^{-1}, lightweight Pt crucible. Insert shows portion of a DTA trace using a more sensitive Δt setting. See text for significance of letters

the type of TG record obtained, the major difference being the presence of an arrest in Fig. 2. The letters refer to the positions on the TG traces at which samples were taken for optical, XRD, SEM and microprobe analysis. Experiments which studied the effects of air flow rate (from 0 to 200 ml/min), particle size (screen size fractions $<37\ \mu m$ to $300-212\ \mu m$) and crucible properties (heat capacity from $6-117\ JK^{-1}\times10^{3}$ and thermal conductivity from $1-72\ Wm^{-1}K^{-1}$) showed that the arrest was only completely absent when the experiments were carried out in silica crucibles, high air flow rates (>120 m/min) and small particle size ($<150\ \mu m$). The silica crucibles had the smallest cross-sectional area (12.6 mm^2) yet yielded the highest maximum rate of weight loss ($1.4\times10^{-5}\ g\ s^{-1}$). When, however, the crucibles were used in stagnant atmospheres, the maximum rate of weight loss was reduced ($7.5\times10^{-6}\ g\ s^{-1}$) and the arrest reappeared. The total weight loss shown in Figs 1 and 2 was 31.9 and 32.5% respectively. These figures agree, within the limits of experimental error, with the theoretical weight loss expected for reaction to hematite of 33.4%.

Reaction, as evidenced by both the TG and DTA traces, became apparent at about 430°. The main feature of the DTA traces was the large exothermic peak which commenced at temperatures between 530 and 550°; this corresponded with the onset of the maximum rate of weight loss on the TG trace. During the period of maximum rate, the measured sample temperature exceeded the programmed temperature the amount (9–29°) depended upon the experimental conditions and the crucible material (silica, platinum or alumina). Figure 2 shows that during the arrest little weight loss occurred for a period of 8 min, during which time the programmed temperature had increased to 620°. The heat effects associated with the arrest were small in relation to those occurring during the main reaction and were endothermic (see insert, Fig. 2).

XRD examination

Quenching of the particles was found to be essential to preserve the phases present at the reaction temperatures. At the commencement of the project, particles were produced for examination by quickly raising the furnace from around the specimen and allowing the crucible to air-cool. It was difficult, unless large samples were taken, to preserve pyrrhotite by this technique, and hematite was invariably found rather than magnetite.

Some of the phases were present in small quantities, e.g., of the order of 5% of the sample weight. In order to detect them it was necessary to use a Guinier focusing powder camera. However, the initial film formed on the pyrite (e.g., corresponding to the position shown as point A on Figs 1 and 2) was too thin to identify by this technique and it was necessary to resort to isothermal experiments in order to produce sufficient thickness of material for identification. Isothermal experiments were accordingly conducted at 430° for 180 min and 460° for 55 min. The phases found in these experiments (position A) and at other temperatures corresponding to various positions along the TG trace are shown in Table 1.

Table 1

XRD analyses of oxidized pyrite (the letters identify the sample positions on Figs 1 and 2)

Position	Phases
A*	pyrite, magnetite, hematite
B	pyrite, pyrrhotite, hematite
C	hematite
D	hematite

* Isothermal test

Quenched specimens similar to those used for the XRD examination were mounted in resin, and polished sections made.

Optical microscopic examination

An optical micrograph made from material from position A is shown in Fig. 3. This micrograph showed the cohesive nature of the initial layer formed on the pyrite surface and along cracks in the grains. From evidence of optical activity, this initial layer (3 – 5 μm thick) appeared to be hematite, in agreement with the results of XRD analysis reported in the preceding section.

Figure 4 shows an optical micrograph corresponding to position B (i.e., at the start of the period of maximum reaction shown on the TG trace). A small amount of pyrrhotite – identified by the creamy colour – was evident at the interface of the pyrite core. The pyrrhotite was not, in most cases, continuous but was characterized by the appearance of local islands and fingers which intruded into the sur-

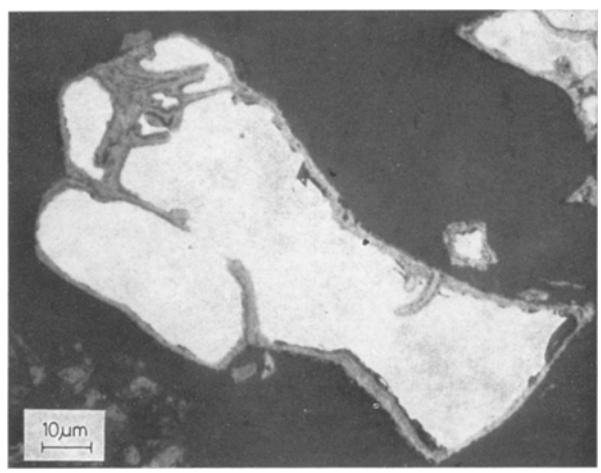

Fig. 3. Optical micrograph corresponding to position A on TG trace

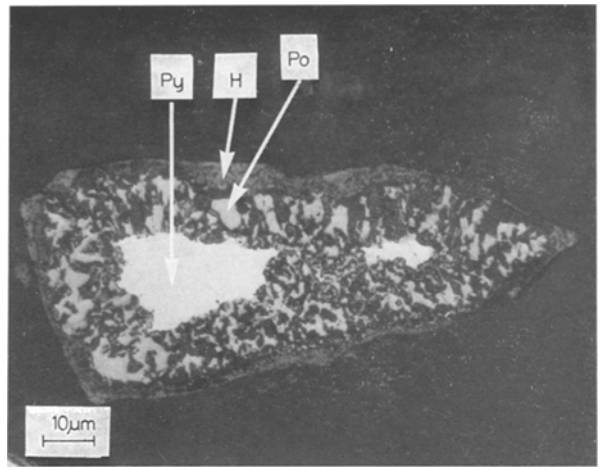

Fig. 4. Optical micrograph corresponding to position B on TG trace. Py = pyrite, Po = pyrrhotite, H = hematite

rounding oxide layer. The porous nature of the oxide should be noted as, too, should the presence of the initial oxide film which was still maintained on the outside of the grains.

The micrographs corresponding to positions C and D were similar; completely reacted material corresponding to position D is shown in Fig. 5. The preservation of the initial oxide layer and the porous nature of the core is again apparent. The optical activity indicated that both the core and the outer skin were hematite. Syn-

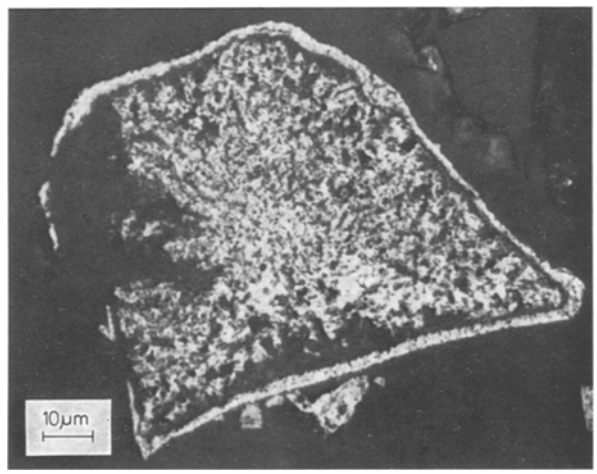

Fig. 5. Optical micrograph corresponding to position D on TG trace

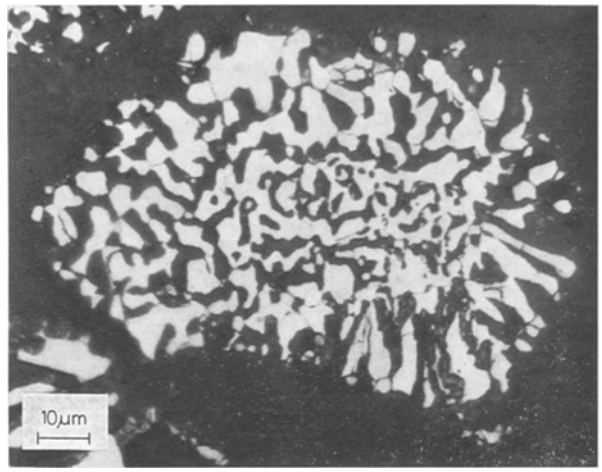

Fig. 6. Optical micrograph showing synthetic pyrrhotite

thetic pyrrhotite was produced by thermally decomposing the pyrite used in the oxidation experiments in an atmosphere of nitrogen. A micrograph showing the porous nature of synthetic pyrrhotite is shown in Fig. 6.

SEM examination

The backscattered electron images were similar to those described in the previous section. Energy dispersive analysis of the X-rays from the polished sections (position B) gave iron to sulphur ratios which confirmed the presence of pyrrhotite around the interface with the pyrite cores. Similar measurements (position C) gave detectable sulphur contents in a narrow band near the outer edge of the oxide layer.

Microprobe examination

Efforts were made to use this technique to distinguish between magnetite and ferric oxide. These attempts were unsuccessful because the varying porosity limited the high degree of accuracy of iron analysis required to make this distinction. The microprobe was of use, however, in confirming the presence of pyrrhotite and of low sulphur concentrations towards the outer edge of grains from position C. Sulphur and iron traverses across a grain are shown in Fig. 7. No sulphur was detected in the outer layer of specimens from position D, i.e., for the fully reacted specimens. The higher sulphur levels near the edge were attributed to the presence of sulphate.

Discussion

Thermodynamic considerations

The usefulness of chemical potential diagrams in aiding the understanding of metallurgical problems has been well illustrated by recent papers by Rosenqvist

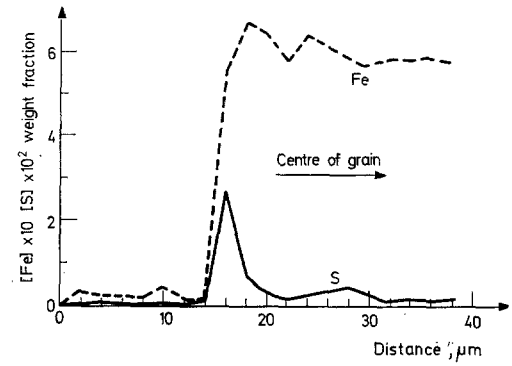

Fig. 7. Microprobe traverses across oxidized pyrite grain corresponding to position C on TG trace

[18] and Yazawa [19]. In this paper, thermodynamic equilibria in the Fe–S–O system were investigated using $\log p_{O_2}$ *vs* $\log p_{S_2}$ diagrams. The data used in the construction of these diagrams came from a number of sources [20–22]. The possibility of anhydrous oxysulphate formation was not considered as there are no published free energy data for these compounds. Two diagrams for 427, and 627° are shown in Figs 8 and 9.

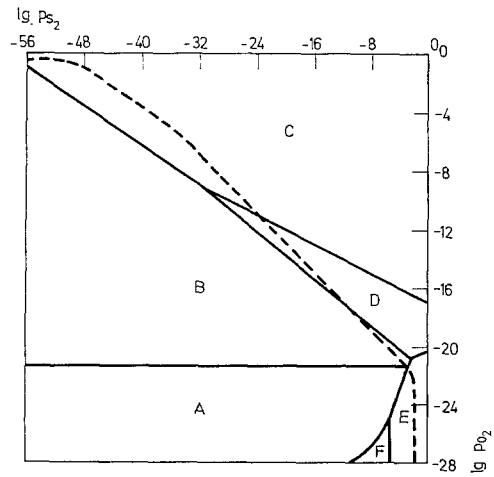

Fig. 8. Sulphur-oxygen potential diagram for Fe–S–O system at 427 °C. Pressure equilibrium line shown dashed. See Fig. 9 for key

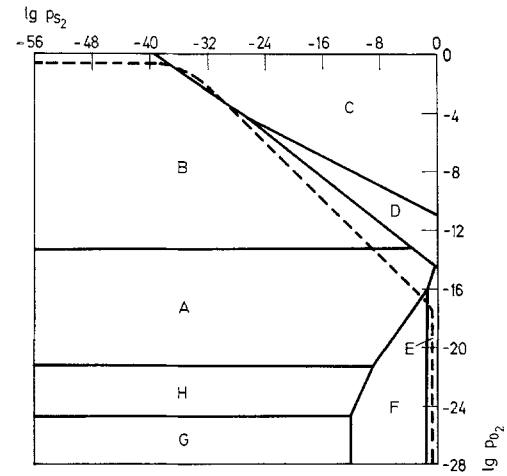

Fig. 9. Sulphur-oxygen potential diagram for Fe–S–O system at 627°. Pressure equilibrium line shown dashed. A = magnetite, B = hematite, C = ferric sulphate, D = ferrous sulphate, E = pyrite, F = pyrrhotite, G = iron, H = wustite

Pressure considerations

The micrographs shown in Figs 4 and 5 show that the oxide formed at temperatures above 530–550° was porous; micrographs presented elsewhere [23] show that the oxide formed at lower temperatures was cracked. Thus, it is likely that the gas phase was continuous through the layers of oxidation product at most times. If pressure equilibrium applies, i.e., no pressure-induced flows, then for oxidation at a total pressure of one atmosphere the equilibrium pressures of the gas components, omitting nitrogen, are related by

$$p_{O_2} + p_{SO_2} + p_{SO_3} + \sum p_{S_n} \approx 0.2 \qquad (1)$$

where $\sum p_{S_n}$ corresponds to the combined pressure of the various gaseous sulphur species. Equilibrium values of the latter were determined from Mills [24] and were used to determine values of p_{S_2} and p_{O_2}, satisfying this equation. These values have been plotted on Figs 8 and 9.

The diagrams show that the likely order of solid phases, proceeding outwards from the pyrite interface, is as in Table 2. It can be seen that wustite formation is highly unlikely. Using graphical procedures, it was shown (for $p_{SO_2} = 0.2$ atm) that

1) below 404° magnetite is not stable and ferric oxide should form directly in contact with pyrite.

2) pyrrhotite becomes a stable phase at temperatures above 552°, and

3) ferrous and ferric sulphate are unstable above 583 and 644° respectively.

Table 2

Predicted phase assemblages

Phases	Temperature, °C	
	427	627
Pyrite	√	√
Pyrrhotite	√	√
Magnetite	√	√
Hematite	—	√
Ferrous sulphate	√	—
Ferric sulphate	√	√
Hematite	√	√

Reconciliation with the phases found in practice

The phases found do not contradict the thermodynamic predictions; we have, however, been unable to find the full range predicted. This probably reflects the inadequacy of the methods of phase identification. Traces of magnetite were only found in the isothermal samples from the lowest temperatures (Table 1). The possibility, however, of a thin layer of magnetite (too thin to be detected by XRD) being present at the higher temperatures should not be discounted. In this regard, it was unfortunate that the microprobe was not able to differentiate between ferric oxide and magnetite.

Due to the small amount in our samples, it was not possible to identify the form of the sulphate. The results, however, are capable of interpretation without postulating the presence of oxysulphates. Our findings, therefore, differ from those of Banerjee [2] who claimed to have identified oxysulphates in the products of oxidation of both natural and synthetic pyrite. His identification was based solely on the results of chemical analysis and it is doubtful whether this method had sufficient precision to identify the small quantity involved (e.g., 4%). Also the natural pyrite used in his tests contained an appreciable amount of ferrous sulphate heptahydrate, and the oxysulphate, if present, may have resulted from the decomposition of this material [25–27].

The ignition temperature of pyrite

The thermodynamic analysis indicated pyrrhotite should become stable at temperatures above 550°. This temperature also approximated the temperature 530–550° previously noted as corresponding to the start of the period of most intense reaction. The presence of pyrrhotite during this phase of the reaction has been confirmed by EDAX and microprobe analysis.

Using the densities quoted in Taggart [28], it can be shown that the oxidation of pyrite to pyrrhotite, magnetite, or hematite results in a reduction in volume of 20.4, 34.8 and 37.8% respectively. At temperatures below 530–550°,

the oxide formed directly on the pyrite surface and the volume mismatch was accommodated by circumferential cracking of the oxide [23]. At higher temperatures pyrrhotite accommodated the 20.4% volume mismatch with pyrite by assuming by porous structure. This is well illustrated by Fig. 6, which shows material produced by the thermal decomposition of pyrite in an inert atmosphere. The porous structure of the pyrrhotite was maintained during further oxidation, albeit with further reduction in volume, through to the final oxide (Fig. 5). The contrast in structure between the low-temperature outer skin of oxide and the internal oxide formed via the intermediate pyrrhotite is clearly evident in Figs 3 to 5.

Other tests [29, 30], in which the combustion of pyrite particles was studied under simulated suspension smelting conditions, gave similar ignition temperatures.

The arrest in the TG traces

We believe that the arrest resulted from the presence of sulphate in the sample. This contention is supported by

1) the evidence of sulphur in the outer oxide layers of specimens from position C,

2) the weight loss remaining constant until the programmed temperature reached 620°. This was approaching the 644° calculated as being the maximum temperature at which ferric sulphate would be stable, and

3) the heat effects associated with the renewed reaction were endothermic – the decomposition of ferrous and ferric sulphate are both endothermic.

In understanding the absence of the arrest in some experiments, it was instructive to consider the heat transfer process operating during the period of maximum rate of reaction. Heat produced in the sample would either be dissipated to the gas, conducted to the crucible or radiated to the surrounds. Under our conditions of point contact of the grains with the crucible and limited access of gas, the latter was likely to be the predominant process. By considering the sample to be a disc in the bottom of the crucible and that steady-state conditions prevail, it was possible to calculate the likely temperature of the sample. Calculated temperatures ranged from 640°, for the highest maximum rate of weight loss (1.4×10^{-5} g s^{-1}) when no arrest was present, to 600° for the stagnant atmosphere experiments which had the lowest maximum rate of weight loss (7.5×10^{-6} g s^{-1}) and which showed an arrest in the TG traces. Thus the presence or absence of the arrest appears to be due to the temperature rise experienced by the sample during the period of most intense reaction. If the temperature exceeds that at which ferric sulphate is stable there is no arrest. If, however, the temperature is not high enough, some sulphate remains and an arrest occurs.

Conclusions

The literature pertaining to the phases formed during the oxidation of pyrite is confusing. There are two reasons for this conflict. (a) Phases have been claimed to be absent when they may have been present; this arises because of the reliance on

powder XRD techniques with a lower detection limit of about 5% for the phase identification. The present work has shown that some phases, notably pyrrhotite and sulphate, were present below this level and demonstrated that other techniques, e.g., EDAX and microprobe, were required for detection. (b) In previous studies, little attempt was made to quench the samples and preserve the phases present at the reaction temperature. In the present work, it was demonstrated that when small samples were used it was essential to quench to preserve pyrrhotite and magnetite. Pyrrhotite was positively identified at temperatures above 530° and at higher temperatures microprobe analyses detected sulphate on a narrow band towards the outer edge of the ferric oxide layer.

Pyrrhotite becomes an intermediate oxidation product above 530–550°. Oxide formed via pyrrhotite is porous and is no longer protective; oxygen has freer access to the unreacted sulphide and intense reaction occurs. This explains the onset of the DTA peak in the records of thermal analysis and ignition under suspension smelting conditions.

Some of the thermal analyses exhibited an arrest in the TG traces, the occurrence of which was thought to be due to sulphate formation. The absence of the arrest from some traces was attributed to the high temperatures attained during the period of maximum reactivity. Calculations indicated that the temperature of samples showing the arrest was about 600° whereas when the arrest was absent, the sample temperature approached 640°, the maximum temperature at which ferric sulphate is stable.

*

The authors gratefully acknowledge the assistance of Drs G. Mumme and R. Segnit and Messrs. I. Harrowfield, A. Holland and J. Watts for assistance with the conduct of the experimental programme.

References

1. V. I. Silaev, A. F. Zaboev, V. I. Ilovaiskii and L. A. Khoroshilova, Tr. Inst. Geol. Komi Fil. Akad. Nauk SSSR, 23 (1977) 88.
2. A. C. Banerjee, Indian J. Chem., 14A (1976) 845.
3. B. Zalar and S. Pirc, Rud-Metal Zb, 2–3 (1976) 247.
4. A. F. Lozhkin, Khim. Khim. Tekhnol. Obl. Nauchno-Tekh. Konf., 4th ed. S. F. Kudryashov 1973, Vol 2., p. 13.
5. E. Iwanciw, M. Krol and B. Szafirska, Zesz. Nauk. Akad. Gorn-Hutn, Cracow Met. Odlew, 44 (1972) 115.
6. J. R. Schorr and J. O. Everhart, J. Am. Ceram. Soc., 52 (1969) 351.
7. J. R. Blachere, J. Am. Ceram. Soc., 49 (1966) 590.
8. O. C. Kopp and P. F. Kerr, Am. Mineralogist, 43 (1958) 1079.
9. R. A. Schoenlaub, J. Am. Ceram. Soc., 52 (1969) 40.
10. C. Maurel, Compt. Rend., 257 (1963) 47.
11. K. Nishihara and Y. Kondo, Mem. Fac. Eng. Kyoto Univ., 21 (1959) 214.
12. K. Niwa and T. Wada, Nippon-Kinzoku-Gakkai-Shi, 18 (1954) 1.
13. G. M. Schwab and J. Philinis, Z. Anorg. Chem., 253 (1945) 71.
14. B. Zalar, J. Wohinz and A. Valant, Zelezarski Zb, 10 (1976) 109.
15. K. Niwa, T. Wada and Y. Shiraishi, AIME Trans., 209 (1957) 269.

16. D. I. RYZHONKOV and P. S. UMANSKII, Kinet. Zakonomern. Sovmestnogo Vosstanov Okislow Zheleza Drugikh Mater, Mosk. Inst. Stali. Splavov, Moscow, (1973) 136.
17. A. N. SPEKTOR, A. D. MARKOV, A. N. PYRIKOV and P. S. UMANSKII, Zh. Prikl. Khim. (Leningrad), 45 (1972) 1713.
18. T. ROSENQVIST, Met. Trans., 9b (1978) 337.
19. A. YAZAWA, Met. Trans., 10b (1979) 307.
20. R. A. ROBIE and D. R. WALDBAUM, Thermodynamic Properties of Minerals and Related Substances at 298.15 °K (25.0 °C) and One Atmosphere Pressure and at Higher Temperatures, U.S. Govt. Printing Office, Washington, 1968.
21. D. R. STULL and H. PROPHET, JANAF Thermochemical Tables, 2nd edn, Office of Standard Reference Data, National Bureau of Standards, Washington, 1971.
22. D. Ribbe, ed., Sulfide Mineralogy, Vol. I, Mineralogical Society of America, Washington, 1974.
23. F. R. A. JORGENSEN and F. J. MOYLE, Met. Trans., 126 (1981) 769.
24. K. C. MILLS, Thermodynamic Data for Inorganic Sulfides, Selenides and Tellurides, Butterworth & Co. Ltd, London, 1974.
25. M. S. R. SWAMY, T. P. PRASAD and B. R. SANT, J. Thermal Anal., 15 (1979) 307.
26. M. S. R. SWAMY, T. P. PRASAD and B. R. SANT, J. Thermal Anal., 16 (1979) 471.
27. A. E. KAMEL, Z. SAWITES, H. KHALIFA, S. A. SALEH and A. M. ABDALLAH, J. Appl. Chem. Biotechnol, 22 (1972) 591.
28. A. F. TAGGART, Handbook of Mineral Dressing, John Wiley & Sons, Inc., New York, 1944.
29. F. R. A. JORGENSEN, Trans. IMM, 90C, (1981) 1.
30. F. R. A. JORGENSEN, Proc. Australas. Instn. Min. Metall., 268 (1978) 47.

ZUSAMMENFASSUNG — Die Oxydation von Pyrit wurde durch thermische Analyse und Abschrecken der in verschiedenen Stadien der Reaktion gebildeten Phasen untersucht. Die Phasen wurden durch optische Mikroskopie, SEM, EDAX, XRD und microprobe-Analyse charakterisiert. Im wesentlichen wurden die unter Annahme des thermodynamischen Gleichgewichts und Druckgleichgewichts vorausgesagten Phasen gefunden. Die Voraussagen waren, daß (1) unter 404 °C Haematit direkt an der Oberfläche des Pyrits gebildet wird, während bei höheren Temperaturen Magnetit auftritt, (2) Pyrrhotit eine stabile Phase oberhalb 552 °C bildet und (3) sich Ferro- bzw. Ferrisulfate in den äußeren Schichten bei Temperaturen unter 583 bzw. 644 °C bilden. Es wurde festgestellt, daß die Entzündungstemperatur des Pyrits derjenigen Temperatur entspricht, bei der die Bildung von Pyrrhotit einsetzt. Eine Stufe in einigen der TG-Kurven wurde der Anwesenheit von Sulfaten zugeschrieben, wobei die An- oder Abwesenheit der Stufe von der Temperaturerhöhung abhängig ist, der die Probe während der Oxydation ausgesetzt ist.

Резюм — С помощью термического анализа изучено окисление пирита и отдельных фаз, образующихся на различных стадиях реакции. Фазы были охарактеризованы оптической микроскопией, СЕМ, ЕДАХ, ХРД и анализом микропробы. Обнаруженные фазы по существу были аналогичны установленным на основе термодинамического равновесия и равновесного давления. Установлено, что ниже 404°С происходит образование гематита прямо на поверхности пирита, а при более высоких температурах примешивается и магнетит. Пирротит становится стабильной фазой выше 552°. При температурах ниже 583° и 644° образуются во внешних слоях сульфаты двух- и трехвалентного железа. Найдено, что температура воспламенения пирита совпадает с началом образования пирротита. Некоторая задержка на ТГ была отнесена за счет присутствия сульфата. Наличие или отсутствие такой задержки зависело от подъема температуры, вызванного окислением образца.